

Heat Transfer in Two-Pass Rotating Rectangular Channels (AR=2) With Five Different Orientations of 45 Deg V-Shaped Rib Turbulators

Luai AL-Hadhrami*

Research Assistant

Todd Griffith

Research Assistant

Je-Chin Han

M.C. Easterling Endowed Chair

e-mail: jchan@mengr.tamu.edu

Turbine Heat Transfer Laboratory,
Department of Mechanical Engineering,
Texas A&M University,
College Station, Texas 77843-3123, USA

An experimental study was made to obtain heat transfer data for a two-pass rectangular channel (aspect ratio=2:1) with smooth and ribbed surfaces for two channel orientations (90 deg and 135 deg with respect to the plane of rotation). The V-shaped ribs are placed on the leading and trailing surfaces. Five different arrangements of 45 deg V-shaped ribs are studied. The Reynolds number and rotation number ranges are 5000–40000, and 0.0–0.21, respectively. The rib height to hydraulic diameter ratio (e/D) is 0.094; the rib pitch-to-height ratio (P/e) is 10; and the inlet coolant-to-wall density ratio ($\Delta\rho/\rho$) is maintained around 0.115 for every test. The results show that the rotation-induced secondary flow enhances the heat transfer of the first pass trailing surface and second pass leading surface. However, the first pass leading and the second pass trailing surfaces show a decrease in heat transfer with rotation. The results also show that parallel 45 deg V-shaped rib arrangements produce better heat transfer augmentation than inverted 45 deg V-shaped ribs and crossed 45 deg V-shaped ribs, and a 90 deg channel orientation produces greater rotating effect on heat transfer than a 135 deg orientation.

[DOI: 10.1115/1.1561455]

Keywords: Enhancement, Finned Surfaces, Heat Transfer, Rotating, Turbines

Introduction

To achieve high thermal efficiency in a gas turbine engine, the turbine inlet gas temperature should be increased. However, the penalty is a high thermal load, which affects the durability of the turbine components. Therefore, improved cooling techniques such as film cooling and internal cooling are applied to turbine blades. Internal cooling is achieved by circulating low enthalpy air in multi-pass flow channels inside the blade structure. To increase the heat transfer of the internal cooling, the internal surfaces usually are roughened by angled ribs to trip the boundary layer and increase turbulence. As the turbine blade rotates, Coriolis and buoyancy forces cause different heat transfer behavior between the leading and trailing surfaces.

Over the past few decades numerous studies have been made experimentally on the flow field and heat transfer in the internal coolant passages of gas turbine rotor blades. Metzger et al. [1] studied forced convection in a non-rotating two-pass smooth rectangular channel by varying the divider location and the gap at the 180 deg turn. Fan et al. [2] extended the Metzger et al. [1] work by varying the channel width and concluded that increasing the channel aspect ratio resulted in smaller azimuthal heat transfer variations and increased overall channel heat transfer. Han and Park [3] performed experimental studies on heat transfer characteristics in a non-rotating rib-roughened rectangular channel. Han et al. [4] studied the effect of the rib angle orientation on heat transfer distributions and pressure drop in a non-rotating square channel with two opposite in-line ribbed walls. They found that the 60 deg and 45 deg V-shaped ribs performed better than the 60 deg and 45 deg parallel ribs and, subsequently, better than the 60

deg and 45 deg crossed ribs and the 90 deg rib. The V-shaped ribs produced the highest heat transfer augmentation, while the crossed ribs had the lowest heat transfer enhancement. Taslim et al. [5] measured heat transfer and friction in channels roughened with angled V-shaped and discrete ribs on two opposite walls. Ekkad and Han [6] performed a detailed study on heat transfer distributions in a non-rotating square ribbed channel using a liquid crystal technique. The results show that the 60 deg, V-shaped ribbed channel produced more heat transfer enhancement than 60 deg and 90 deg angled ribbed channels. Kiml et al. [7] investigated heat transfer enhancement mechanisms in a rectangular channel with V- and Λ -shaped ribs. They used a flow visualization technique to examine the secondary flow behaviors created by the V-shaped ribs.

Recently, experiments with rotation have been conducted to closely model turbine blade cooling environments. Wagner et al. [8,9] conducted a detailed experimental study to determine the effects of rotation (buoyancy and Coriolis forces) on the local heat transfer of a multi-pass square channel with smooth walls. They concluded that in the first pass with radially outward flow, rotation created a thinner boundary layer with higher heat transfer on the trailing surface and a thicker boundary layer with lower heat transfer on the leading surface. In the second pass with radially inward flow, opposite heat transfer results were obtained. Johnson et al. [10,11] performed a systematic investigation of the effects of buoyancy and Coriolis forces on the heat transfer coefficient distribution of a four-pass square channel with 45 deg ribs angled to the flow. They concluded that both the rotation and channel orientation with respect to the axis of rotation could change the leading and trailing surface heat transfer coefficients of the ribbed channel. Han et al. [12] investigated an uneven wall temperature effect on local heat transfer in a rotating two-pass square channel with smooth walls. Zhang et al. [13] analyzed the heating condition effects in a two pass square channel with 60 deg angled rib

*Current address: Assistant Professor, King Fahd University, Saudi Arabia.

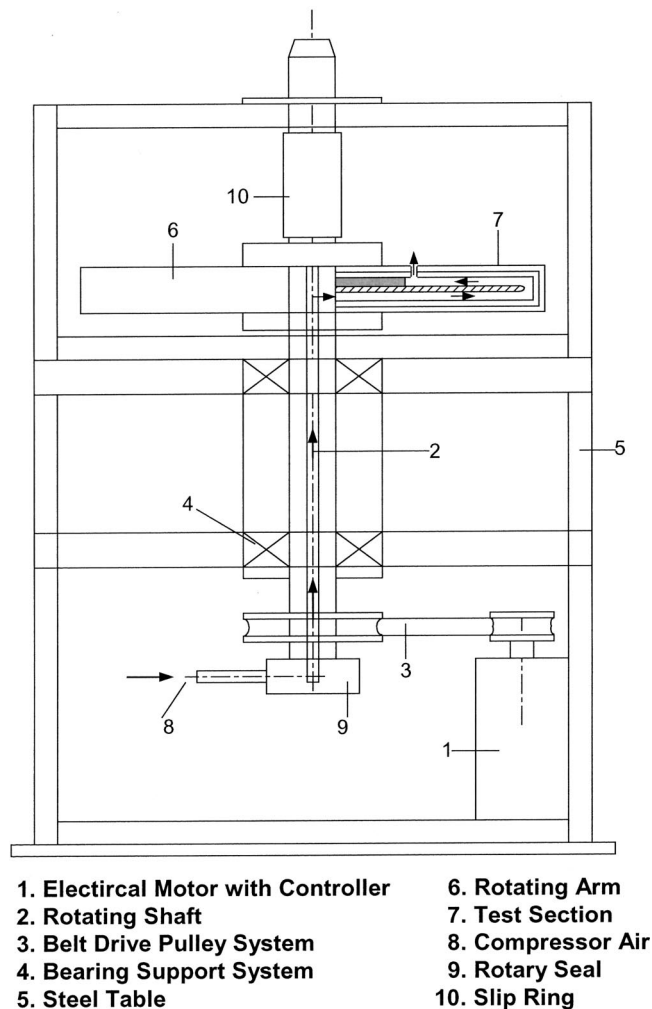
Contributed by the Heat Transfer Division for publication in the JOURNAL OF HEAT TRANSFER. Manuscript received by the Heat Transfer Division January 25, 2002; revision received November 8, 2002. Associate Editor: H. S. Lee.

turbulators with rotation. They suggested that an uneven wall temperature had a significant impact on the local heat transfer coefficients. Parsons et al. [14,15] studied the effects of channel orientation and wall heating condition on the local heat transfer coefficient in a rotating two-pass square channel with ribbed walls. They found that the effects of the Coriolis force were reduced as the channel orientation changed from a normal ($\beta=90$ deg) to an angled orientation ($\beta=135$ deg). Dutta and Han [16] also investigated the local heat transfer coefficients in rotating smooth and ribbed two-pass square channels with three channel orientations. Dutta et al. [17] presented experimental heat transfer results for turbulent flows through a rotating two-pass rib-roughened triangular channel, with two channel orientations with respect to the direction of rotation. Taslim et al. [18,19] studied the heat transfer characteristics in rib-roughened square and rectangular orthogonal rotating channels. They used a liquid crystal technique to study the effect of rotation on heat transfer distributions on the walls. They found that rotational effects were more pronounced in rib-roughened channels, with a higher channel aspect ratio and a lower rib blockage ratio. Prabhu and Vedula [20] investigated the pressure drop distribution in a rotating rectangular channel with transverse ribs on one wall. They found that a rib array with a pitch-to-height ratio of 5 caused the largest pressure drop. In addition, Park et al. [21] conducted experimental work using Naphthalene sublimation to study the effects of the Coriolis force, 180 deg turn, channel orientation, and the different rib arrangements on local heat/mass transfer distributions on the leading and trailing walls of a two-pass square channel. Azad et al. [22] experimentally investigated the heat transfer distribution in two-pass rotating rectangular channels ($AR=2:1$) connected by a 180 deg turn. The results showed that parallel 45 deg angled ribs produced higher heat transfer distribution than crossed 45 deg angled ribs. For a more comprehensive compilation of turbine blade cooling research, please see the book by Han et al. [23].

Following the above-mentioned research, few papers can be found in the open literature studied the rectangular cross section channel with rotation condition. Hence, the first aim was to study two pass rectangular channels ($AR=2:1$) that are connected by a sharp 180 deg turn. The second motivation was to find different rib configurations that trip the boundary layer and promote more heat transfer inside the two-pass rectangular channels. However, it was found from a previous study by Han et al. [4] that the 45 deg V-shaped ribs show higher heat transfer performance in a one-pass non-rotating square duct compared to other rib configurations (45 deg angled ribs or transverse 90 deg ribs). Thus, we have chosen 45 deg V-shaped ribs to be placed on the leading and trailing surfaces of the two-pass rotating rectangular channels since they have shown a potential for higher heat transfer enhancement. A comprehensive study was conducted to cover five different arrangements of 45 deg V-shaped ribs and a comparison with 45 deg V-shaped crossed rib case. In addition, the effect of the channel orientation with respect to the axis of rotation was investigated for two positions $\beta=90$ deg and $\beta=135$ deg. Such experimental data is not available in the open literature. Our research shows the combined effect of the 45 deg V-shaped rib induced secondary flow and rotation induced secondary flow on the heat transfer distribution in the two-pass rectangular cross-sectional channels.

Description of the Experiment

The experimental test rig used by Azad et al. [22] is employed in this study. Figure 1 shows the schematic of the experimental test rig. Compressed air goes through a filter and an orifice meter, then passes through a rotary seal and a hollow-rotating shaft to feed the test section. The test section is mounted in a horizontal plane. Air travels outward in the first pass and inward in the second pass, and then exhausts into the atmosphere. Slip rings transfer thermocouple outputs to the data logger and power input from transformers to strip heaters, which are fixed under the copper



- | | |
|-------------------------------------|-------------------|
| 1. Electrical Motor with Controller | 6. Rotating Arm |
| 2. Rotating Shaft | 7. Test Section |
| 3. Belt Drive Pulley System | 8. Compressor Air |
| 4. Bearing Support System | 9. Rotary Seal |
| 5. Steel Table | 10. Slip Ring |

Fig. 1 Schematic of the rotating test rig

plates. An electric motor with an adjustable frequency controller rotates the test section. A digital photo tachometer measures the rotational speed of the rotating shaft.

Figure 2 shows a cross sectional view of the test section. The test section has two passes. Each pass is 12.7 mm by 25.4 mm in cross section. The first pass starts with an unheated nylon entrance channel to establish a fully developed flow at the entrance to the heated channel. It has twelve (12) hydraulic diameter lengths to achieve the task. The heated channel length-to-hydraulic diameter (L/D) ratio is 18, while each pass length-to-hydraulic diameter (L/D) ratio is 9, connected by a sharp 180 deg turn. The ratio of the mean rotating arm radius to the channel hydraulic diameter (R/D) is 30. The flow in the first pass is radially outward and the flow in the second pass is radially inward. The heated section is divided into twelve longitudinal sections, six sections in the first pass and six in the second pass, to obtain regionally average heat transfer coefficients. Each longitudinal section has four copper plates on four walls (one per wall) of the channel. Each copper plate is surrounded circumferentially by a thin nylon strip that has a 1.59 mm thickness for insulation from neighboring plates. The copper plates are mounted in a nylon substrate, which comprises the bulk of the test section. Pre-fabricated flexible heaters are installed beneath the leading and trailing surfaces. The side walls are each heated by a wire-wound resistance heater, which is also installed beneath the copper plates. All heaters supply steady, uniform heat flux to the copper plates. Sufficient power is supplied in order to maintain a maximum wall temperature of nearly 65 deg for the corresponding section. This corresponds to an inlet

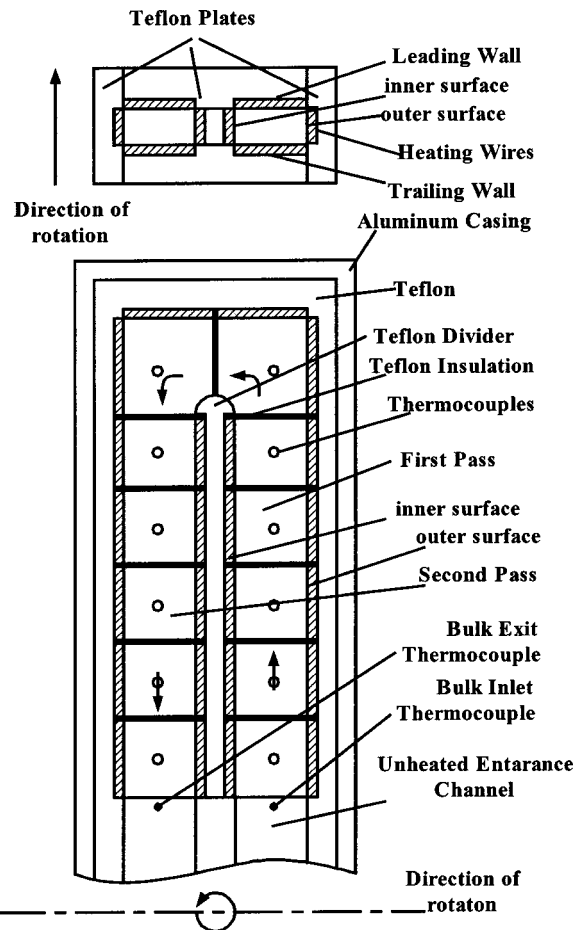


Fig. 2 Cross sectional view of the two-pass rectangular test section

coolant-to-wall density (temperature) ratio ($\Delta\rho/\rho$) of 0.115 for every test. Each 1/8 in. (0.318 cm) thick copper plate has a 1/16 in. (0.159 cm) deep blind hole drilled into its backside in which a copper-constantan thermocouple is installed 1/16 in. (0.159 cm) from the plate surface with thermal conducting glue. The inlet and exit bulk temperatures are measured by thermocouples. The 45 deg V-shaped ribs with a square cross section are made of brass and are glued on the wider walls (leading and trailing surfaces) of the rotating channel. A thin layer of conductive glue is used so that it creates a negligible thermal insulation effect between the brass ribs and the copper plates. The rib-increased surface area is 25 percent with respect to the smooth wall. The entire test duct is surrounded by insulating nylon material and fits in a hollow cylindrical arm for structural rigidity.

Data Reduction

The local heat transfer coefficient is calculated from

$$h = q_{\text{net}} / [A(T_w - T_{bx})] \quad (1)$$

Local net heat transfer rate is the electrical power generated from the heater ($q = VI$) minus losses. Losses were determined by supplying electrical power to the test section until a steady state condition is achieved for a no flow (without any airflow) condition. This is done for several power inputs to obtain a relation between the total heat loss from each surface and the corresponding surface temperature. To place the results on a common basis, the heat transfer area used in Eq. (1) was always that of a smooth wall. The local wall temperature is obtained from thermocouples that impinged in each copper plate. The bulk mean air temperatures

entering and leaving the test section are measured by thermocouples. The local bulk mean temperature (T_{bx}) used in Eq. (1) is calculated from the linear interpolation between the measured inlet and exit air bulk temperatures. The bulk mean temperature rise at the lowest Reynolds number is around 20 deg. Another way to find the local bulk mean air temperature is determined by marching along the test section and calculating the temperature rise from the local net heat input through each set of four heated surfaces. The difference between the calculated and measured outlet bulk mean temperature is between 1–2 deg in all of the cases.

Local Nusselt number is normalized by the Nusselt number for the fully developed turbulent flow in a smooth stationary circular pipe to reduce the influence of the flow Reynolds number on the heat transfer coefficient. Local Nusselt number normalized by the Dittus-Boelter/McAdams correlation is:

$$\text{Nu}/\text{Nu}_o = (hD/K) / [0.023^* \text{Re}^{0.8} \text{Pr}^{0.4}] \quad (2)$$

The Prandtl number (Pr) for air is 0.71. Air properties are taken based on the mean bulk air temperature.

The uncertainty of the local heat transfer coefficient depends on the uncertainties in the local wall and bulk air temperature difference and the net heat input for each test run. The uncertainty increases with the decrease of both the local wall to bulk air temperature difference and the net heat input. The temperature uncertainty is around 0.5 deg. The flowrate uncertainty is less than 4 percent. Based on the method described by Kline and McClintock [24], the typical uncertainty in the Nusselt number is estimated to be less than 9 percent for Reynolds number larger than 10,000. The maximum uncertainty, however, could be up to 23 percent for the lowest heat transfer coefficient at the lowest Reynolds number tested ($\text{Re} = 5000$).

Results and Discussion

Figure 3 shows the 45 deg angled rib that was divided at the centerline to make the 45 deg V-shaped rib. There are two different orientations of the V-shaped rib. The first orientation is called the 45 deg V-shaped rib and the second orientation is called the inverted 45 deg V-shaped rib. Figure 3 also shows the conceptual view of secondary flow induced by the 45 deg angled rib, the 45 deg V-shaped rib, and the inverted V-shaped rib. The 45 deg angled rib induces a secondary flow that moves parallel to the rib from the left side to the right side and returns back to the left side making a counter rotating vortex. The conjectured counter rotating vortex induced by the 45 deg angled ribs has been confirmed from numerical calculations by Al-Qahtani et al. [25].

It is further conjectured that the 45 deg V-shaped rib creates two counter rotating vortices. As the fluid approaches the

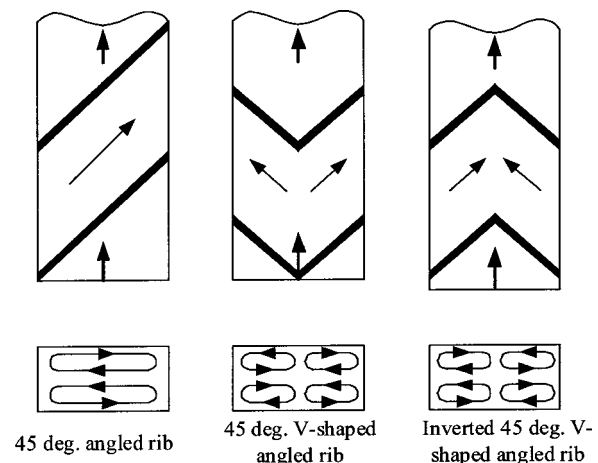


Fig. 3 Conceptual view of secondary flow vortices induced by 45 deg angled ribs and 45 deg V-shaped ribs

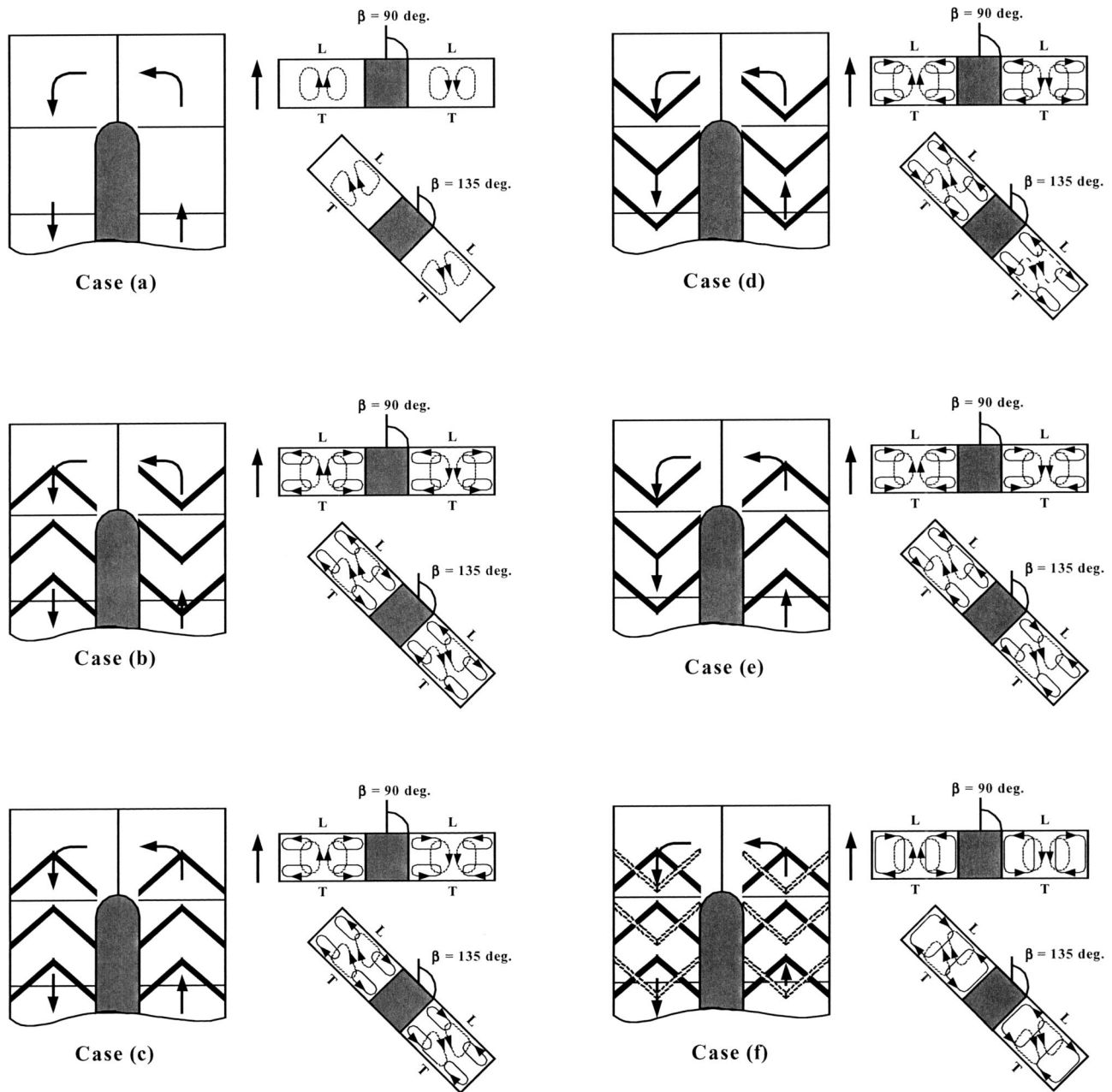


Fig. 4 Conceptual view of the secondary flow vortices induced by rotation, ribs, and channel orientation (dash line: rotation-induced vortices, solid line: rib-induced vortices)

V-shaped rib, it splits into two streams. Each one moves parallel to the rib from the centerline to either the left side or the right side and returns back to the centerline making a counter-rotating vortex. Another observation can be drawn that as the 45 deg V-shaped rib is half the 45 deg angled rib, the boundary layer thickness for the fluid that moves parallel to one side of the 45 deg V-shaped rib is thinner than produced by the 45 deg angled rib. Therefore, since the 45 deg V-shaped rib produces two counter rotating vortices that promote more mixing in the bulk main stream and at the same time produce a thinner boundary layer near the heated surface, a higher heat transfer rate is expected when compared to the 45 deg angled rib. However, a different situation can be observed in the inverted 45 deg V-shaped rib. As the fluid approaches the near surface of the inverted 45 deg V-shaped rib, it starts moving simultaneously from the left side and right side to the centerline, interacting with each other, and then returns back to the starting positions creating two counter rotating vortices. The vortices' in-

teraction may weaken the two counter rotating vortices. Thus, the 45 deg V-shaped rib is expected to perform better than the inverted 45 deg V-shaped rib in the non-rotating condition.

Figure 4 shows conceptual views for the secondary flow patterns of a smooth and ribbed rotating two-pass rectangular channel. Figure 4(a) shows the smooth channel that rotates at $\beta=90$ deg with respect to the direction of rotation. Two symmetrical cells of counter rotating secondary flow (dotted line) appear due to the Coriolis force. In the first pass of the channel, the fluid moves in a radially outward direction, and the effect of the Coriolis force directs the coolant from the core toward the trailing surface. This causes an increase of the heat transfer from the trailing surface and a decrease in the heat transfer from leading surface. However, in the second pass, the opposite situation can be seen: the fluid moves in a radially inward direction, and the Coriolis force directs the coolant toward the leading surface, causing an increase of heat transfer from the leading surface and a decrease in the heat trans-

fer from trailing surface. When the channel is positioned at the $\beta=135$ deg orientation, the secondary flow vortices are asymmetric and migrate diagonally away from the corner region of the inner-leading surface toward the center in the first passage, and from the corner region of the inner-trailing surface toward the center in the second passage.

Figures 4(b) through 4(e) show four different arrangements of the parallel 45 deg V-shaped ribs. These parallel arrangements are attached to leading and trailing surfaces in a parallel fashion so that they are directly opposite to each other. Figure 4(b) shows that the 45 deg V-shaped ribs are attached to the leading and trailing surfaces in both passes. Also, it shows the secondary flow (dotted line) induced by rotational forces and the secondary flow (solid line) induced by the 45 deg V-shaped ribs. As the channel angle changes to $\beta=135$ deg, the rib secondary flow is unchanged, but the rotational secondary flows are shared between the principle surfaces (trailing, and leading) and side surfaces. Figure 4(c) shows the same channel except that the first pass rib orientation is reversed to become inverted 45 deg V-shaped ribs to the mean stream flow. Consequently, all secondary flows that are induced by rotational forces or ribs are the same as case (b) except the rib secondary flow in the first pass is reversed due to the changing in the rib orientation in the first pass. For case (d), as seen in Figure 4(d), the first pass has 45 deg V-shaped rib, and the second pass has inverted 45 deg V-shaped rib. Figure 4(e) shows the first pass and second pass to have inverted 45 deg V-shaped.

Figure 4(f) shows the crossed rib case (the ribs on the leading and trailing surfaces of the cooling channels are in crossed orientation). The crossed orientation of the 45 deg V-shaped ribs coalesces the two pairs of counter rotating vortices into one pair of counter rotating vortices. This reduction in number of rib-induced secondary flow vortices limits the mixing between the near wall flow (hot fluid) and the core flow (cold fluid), which causes less heat transfer. In case of rotation, a pair of rotating-induced secondary flow vortices appears and moves in the opposite direction the vortices generated by crossed ribs. This negative interaction minimizes the rotation effect by suppressing flow impingement on the first pass trailing and second pass leading surfaces and restricts mixing with the core for both leading and trailing surfaces in both passes, which causes low heat transfer enhancement.

Figures 5–10 show the regionally average Nusselt number ratios (Nu/Nu_0) from leading and trailing surfaces for four Reynolds number (5000, 10000, 25000, 40000), rotating and non-rotating, and two channel orientations ($\beta=90$ deg, 135 deg).

Smooth Case Results. Figure 5 shows the results of Nusselt number ratios from leading and trailing surfaces for the smooth case. For the stationary case, the Nusselt number ratio decreases monotonically for both leading and trailing surfaces in the first pass. This continuous decrease is due to the developing thermal boundary layer. As the flow approaches the 180 deg turn, the Nusselt number increases due to secondary flows induced by the 180 deg turn. The Nusselt number reaches the peak value at the entrance of the second pass and then decreases as the flow moves to the exit of the second pass. This is due to the diminishing of the 180 deg turn-induced secondary flows. However, in the rotation case, the Nusselt number ratios from the first pass trailing and second pass leading surfaces are higher than in the non-rotating case, while those from the first pass leading and second pass trailing surfaces are lower. This is due to the rotation-induced secondary flow vortices as shown in Fig. 4(a). At channel orientation $\beta=90$ deg, rotational secondary flow vortices produced by the Coriolis forces are impinging normally on the trailing surface of the first pass and the leading surface of the second pass. However, at channel orientation $\beta=135$ deg, the rotation secondary flow vortices are impinging on the first pass trailing-side corner and the

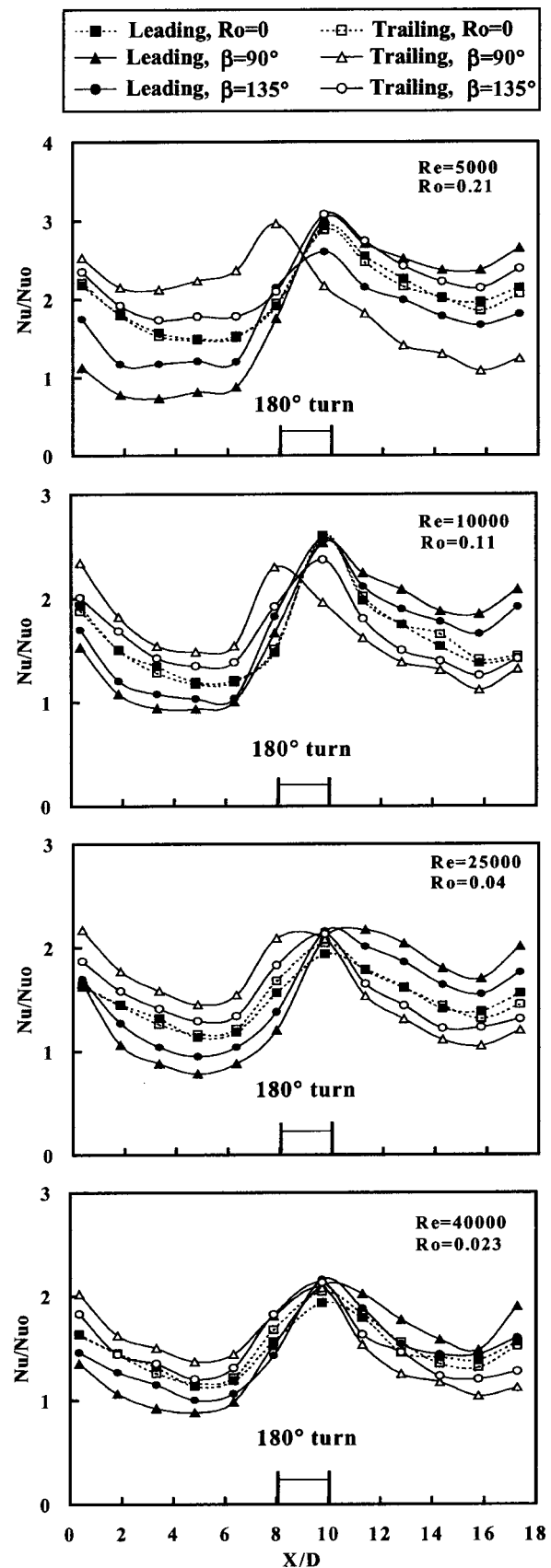


Fig. 5 Nusselt number ratio distribution for case (a)

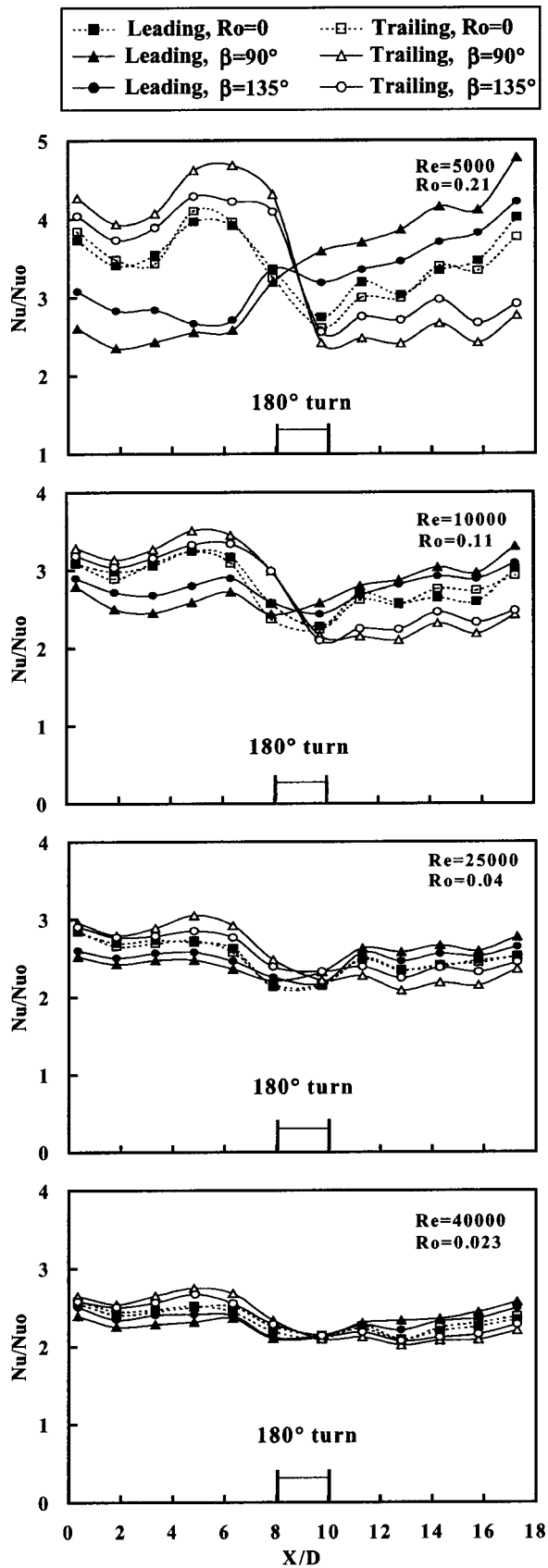


Fig. 6 Nusselt number distribution for case (b)

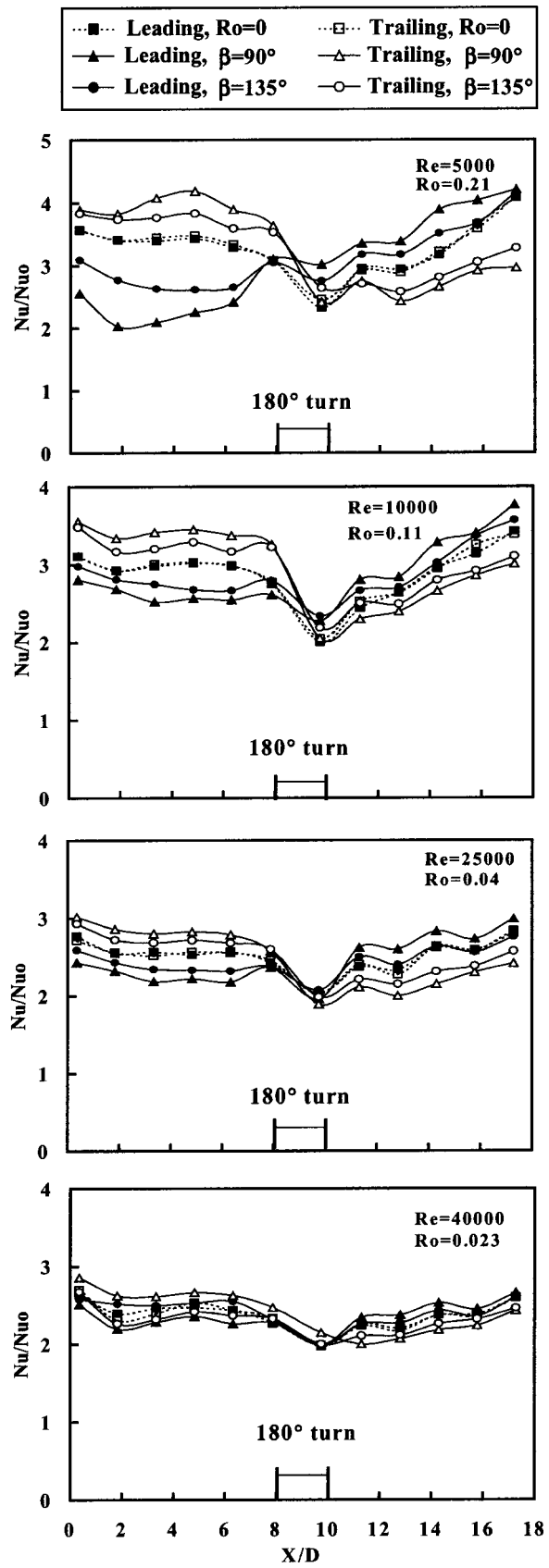


Fig. 7 Nusselt number distribution for case (c)

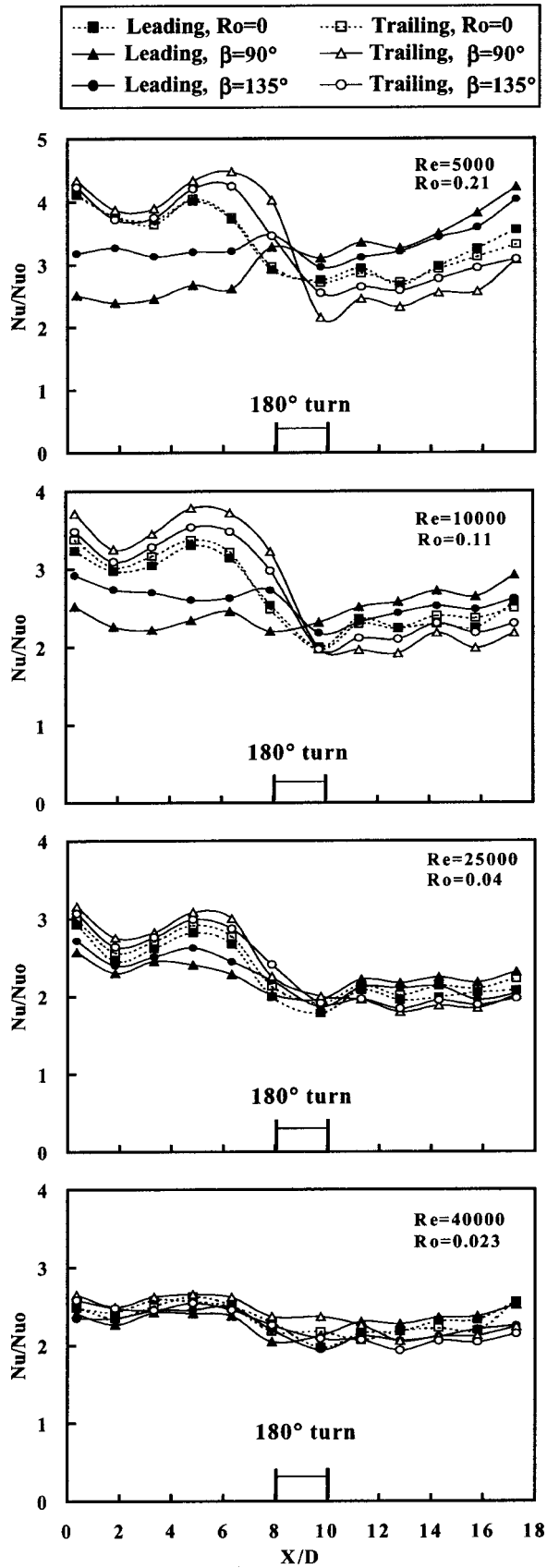


Fig. 8 Nusselt number distribution for case (d)

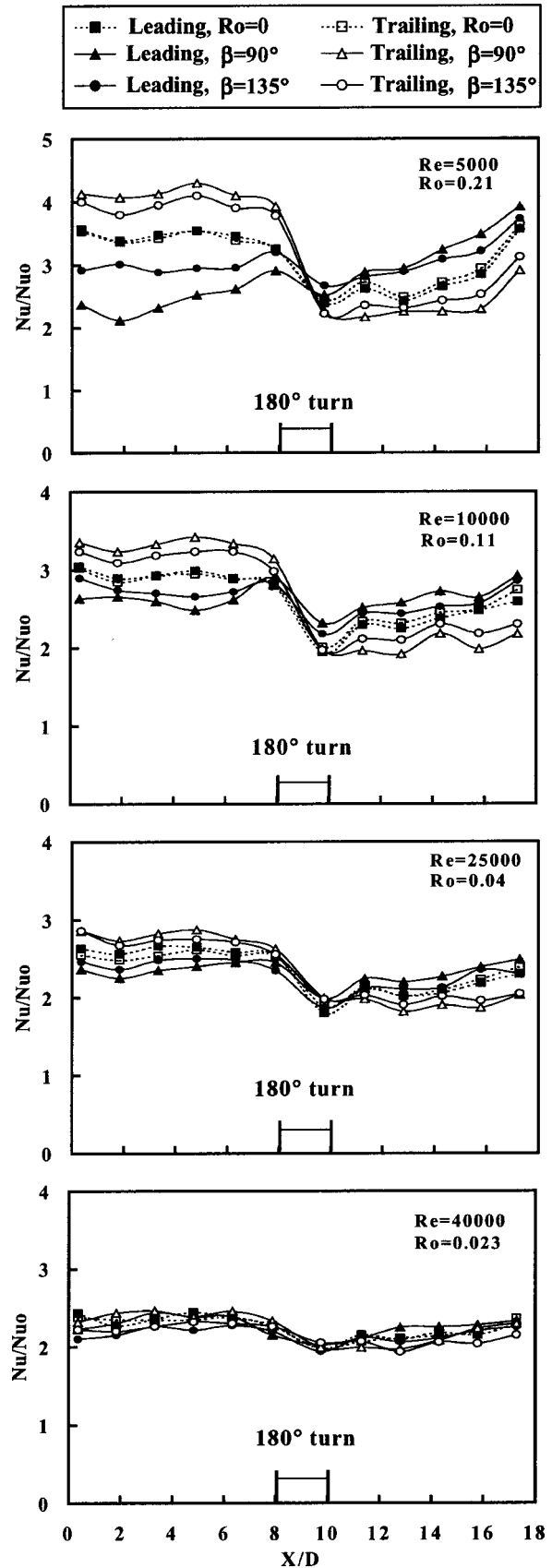


Fig. 9 Nusselt number distribution for case (e)

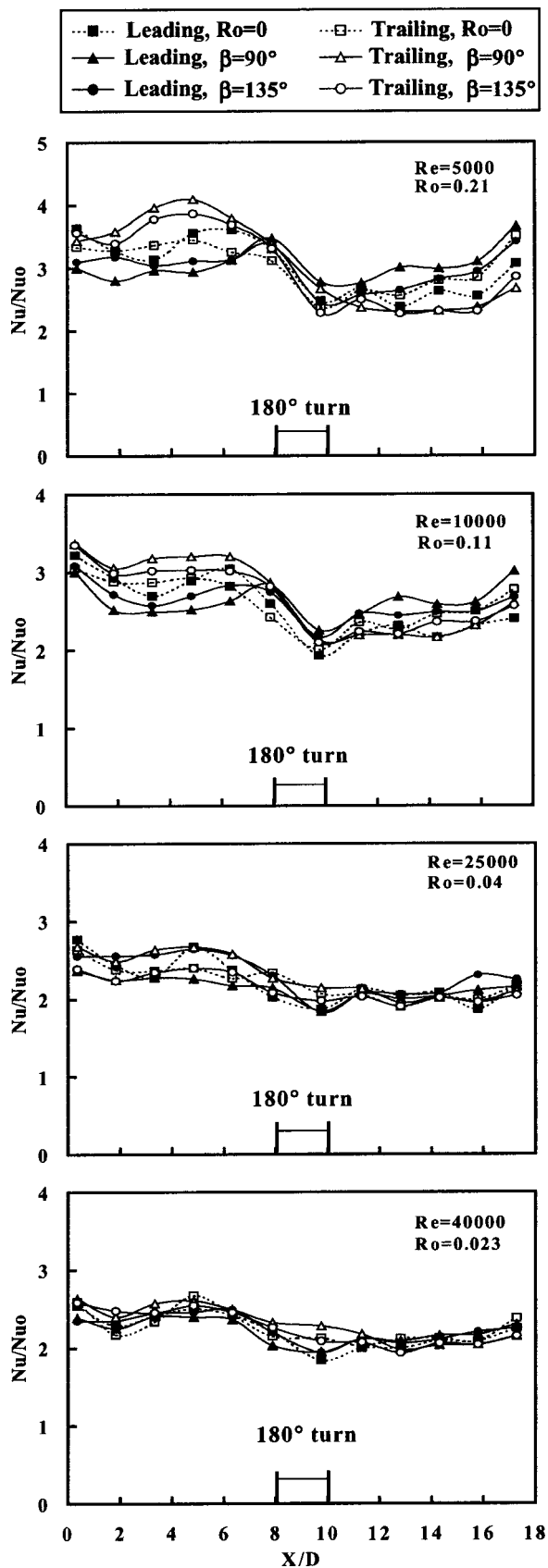


Fig. 10 Nusselt number distribution for case (f)

second pass leading-side corner, as shown in Fig. 4(a). Thus, the Nusselt number ratio for the trailing surface of the first pass and the leading surface of the second pass for channel orientation $\beta=135$ deg are lower than the ratios for channel orientation $\beta=90$ deg. The opposite situation is observed in the leading surface of the first pass and the trailing surface of the second pass. The results also show that the effect of rotation decreases with increasing Reynolds number (or decreasing rotation number). The above-mentioned results are consistent with the previous study (see Azad et al. [22]).

Parallel 45 deg V-Shaped Rib Cases. Figure 6 shows the Nusselt number distribution for case (b). The stationary case results show that the peak Nusselt number ratio occurs at the downstream location of the inlet rather than at the entrance region of the first pass as in the smooth case. This is due to the two pairs of counter rotating secondary flow vortices that are generated by the parallel 45 deg V-shaped ribs, as shown in Fig. 4(b). But, the Nusselt number ratio decreases as the vortices are suppressed by the 180 deg turn. Then, the Nusselt number ratio increases again downstream of the second pass inlet as the secondary flow vortices induced by the parallel 45 deg V-shaped ribs start to develop.

The results show that rotation significantly increases the Nusselt number ratio on the first pass trailing surface and the second pass leading surface, but significantly decreases the Nusselt number ratio on the first pass leading and second pass trailing surfaces. This is because of the combined effect of the rib-induced secondary flow and the rotation-induced secondary flow vortices, as explained in Fig. 4(b). The results of the 135 deg channel also show that rotation enhances the heat transfer in the first pass trailing and second pass leading surfaces, whereas the heat transfer decreases in the first pass leading and second pass trailing surfaces. However, the differences in Nusselt number ratios between leading and trailing surfaces are not as significant for the 135 deg orientation as they are for the 90 deg orientation as explained in Fig. 4(b). The results also show that the rotational effect decreases with an increasing Reynolds number (or decreasing rotation number).

Figure 7 shows the Nusselt number ratio for case (c). Case (c) is generated from case (b) by changing the parallel 45 deg V-shaped ribs in the first pass of case (b) to inverted 45 deg V-shaped ribs. The stationary results show that the first pass Nusselt number ratio behaves differently from that in case (b) at lower Reynolds numbers. This is because, as shown in Fig. 4(c), the inverted 45 deg V-shaped rib vortices tend to interact with each other and reduce the surface heat transfer enhancement. However, the effect diminishes at higher Reynolds numbers. The second pass behavior is similar to case (b) due to the same V-shaped orientation. The results also show that the rotation effect decreases with an increasing Reynolds number (or decreasing rotation number).

Figure 8 shows the Nusselt Number ratio for case (d). In case (d), as explained in Figure 4(d), the Nusselt number ratio distribution in the first pass case (d) is similar to the case (b) first pass because they both have parallel 45 deg V-shaped ribs. In the second pass of case (d), inverted 45 deg V-shaped ribs were placed. The Nusselt number distribution shows lower values compared to the case (b) or case (c) second passes, which have parallel 45 deg V-shaped ribs.

Figure 9 shows the Nusselt number distribution for case (e). Both passes have inverted 45 deg V-shaped ribs as explained in Figure 4(e). The Nusselt number distribution in the first pass is similar to the Nusselt number distribution in the first pass of case (c) and the Nusselt number distribution in the second pass is similar to the Nusselt number distribution in the second pass of case (d).

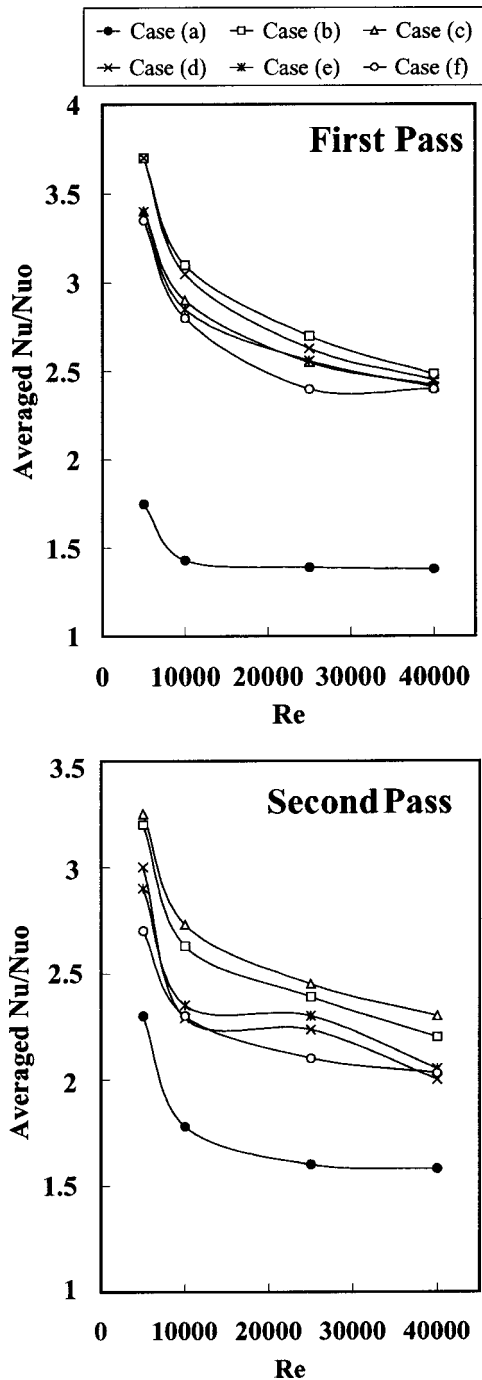


Fig. 11 Averaged Nusselt number distribution for non-rotating ($\omega=0$) cases

Crossed 45 deg V-Shaped Rib Case. Figure 10 shows the Nusselt number distribution for the crossed rib case as can be seen in Figure 4(f). The results show that the non-rotating Nusselt number ratios are unlike the parallel rib case results. Both leading and trailing surfaces show different Nusselt number ratio distributions in each pass. This variation is due to the different orientations of the 45 deg V-shaped ribs that are placed on the leading and trailing surfaces. Their Nusselt number ratios are lower than those of all previous parallel and inverted 45 deg V-shaped rib cases, as explained in Fig. 4(f).

Channel-Averaged Nusselt Number Ratio. Figure 11 presents the averaged Nusselt number ratio distribution for smooth

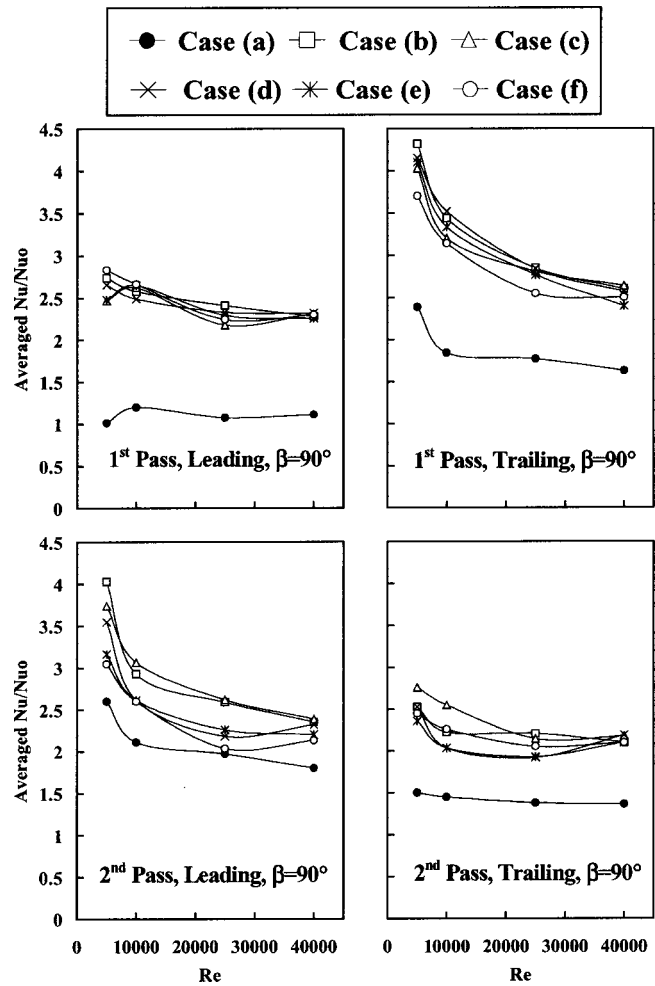


Fig. 12 Averaged Nusselt number distribution for leading and trailing surfaces with rotation ($\omega=550$ rpm) for $\beta=90$ deg

and five different arrangements of the 45 deg V-shaped ribs in the two pass rectangular channels for the stationary case. The Nusselt number ratios in Fig. 11 are the average values of the leading and trailing surfaces for all cases. The results show that the ribbed surfaces provide higher Nusselt number ratios in both passes compared to the smooth surfaces. In the first pass, case (b) and case (d) show higher averaged Nusselt number ratios compared to case (c) and case (e). This is because the 45 deg V-shaped rib induces a stronger secondary flow than the inverted 45 deg V-shaped rib. In the second pass, case (b) and case (c) show better averaged Nusselt number ratios compared to other cases due to the same reason. The crossed V-shaped rib case (f) results show lower averaged Nusselt number ratios compared to the parallel V-shaped rib cases. The crossed V-shaped ribs induce a pair of counter rotating vortices, while the parallel V-shaped ribs induce two pairs of counter rotating vortices, which promote more mixing with the core flow.

Figure 12 shows the channel averaged Nusselt number ratio with respect to Reynolds number for $\omega=550$ rpm on each pass leading and trailing surfaces for $\beta=90$ deg. All Nusselt number ratio results exhibit a decreasing trend with increasing Reynolds number. Ribbed cases provide better Nusselt number ratio enhancement compared to the smooth case. In general, Nusselt number ratios in the first pass leading surfaces are about the same for all V-shaped cases. However, Nusselt number ratios for the V-shaped rib cases (b) and (d) are higher than other cases in the first pass trailing surfaces. A noticeable variation can be seen in the second pass due to the 180 deg turn effect. Cases (b) and (c) of

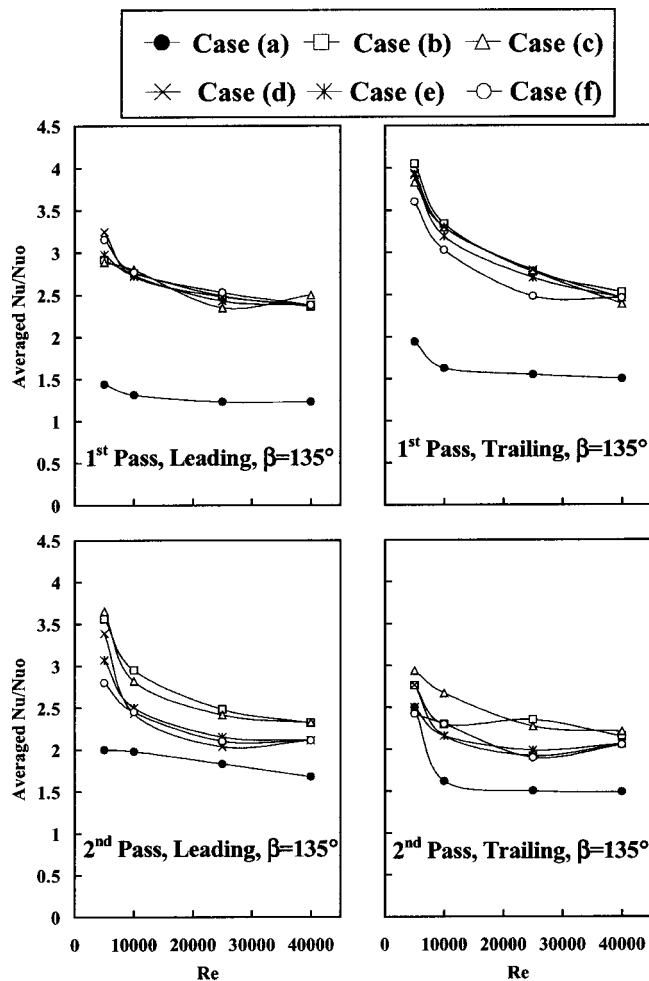


Fig. 13 Averaged Nusselt number distribution for leading and trailing surfaces with rotation ($\omega=550$ rpm) for $\beta=135$ deg

the V-shaped rib show greater values of Nusselt number ratios than cases (d), (e), and (f) (the inverted V-shaped rib and crossed rib).

Figure 13 shows the channel averaged Nusselt number ratio on the leading and trailing surfaces for $\beta=135$ deg. The results are similar to $\beta=90$ deg in trend except that the Nusselt number ratios on the first pass trailing and the second pass leading are lower because of the oblique angle of the flow impinging on the surfaces.

Conclusions

The influences of 45 deg V-shaped rib arrangements and channel orientation on the leading and trailing Nusselt number ratios in a two-pass rectangular channel have been reported for rotation numbers from 0 to 0.21 and Reynolds numbers from 5000 to 40000. The findings are:

1) The general trend of the rotation effect shows an increase in the Nusselt number ratio in the first pass trailing surface and second pass leading surface, while the opposite situation can be observed in the first pass leading surface and second pass trailing surface. This is due to the Coriolis and buoyancy forces, which are generated by rotation. However, the differences between the Nusselt number distributions on the second pass leading and trailing surfaces are smaller than that of the first pass due to the opposite effects of the Coriolis and buoyancy forces.

2) The effects of the Coriolis force and cross-stream flow are reduced as the channel orientation changes from $\beta=90$ deg to $\beta=135$ deg. Thus, the Nusselt number ratios for the $\beta=135$ deg

first pass trailing and second pass leading surfaces decrease when compared to their corresponding Nusselt number ratios for the $\beta=90$ deg orientation. The Nusselt number ratios for $\beta=135$ deg first pass leading and second pass trailing surfaces increase when compared to their corresponding Nusselt number for $\beta=90$ deg.

3) Both orientations of the 45 deg V-shaped rib induce two pairs of counter rotating vortices, but the inverted 45 deg V-shaped rib vortices tend to interact with each other. Therefore, the 45 deg V-shaped rib results in better heat transfer enhancement than the inverted 45 deg V-shaped rib for both non-rotating and rotating conditions.

4) The parallel 45 deg V-shaped rib arrangements provide a higher heat transfer enhancement compared to the crossed 45 deg V-shaped rib arrangement for both rotating and non-rotating conditions. The crossed rib arrangement shows less rotational effect compared to the parallel rib cases. This is because the parallel 45 deg V-shaped rib develops two pair of counter rotating vortices of secondary flows, while the crossed 45 deg V-shaped rib develops only one single pair of counter rotating vortices.

5) For all cases studied here, results show relatively low heat transfer enhancement in the 180 deg turn region. This is because the vortices induced by the V-shaped rib are suppressed by the 180 deg turn and there is no 45 deg V-shaped rib placed at the middle of the 180 deg turn.

6) For all cases studied here, results show that the heat transfer enhancement decreases with increasing Reynolds number.

Acknowledgments

The leading author, Luai AL-Hadhrani, received a fellowship from King Fahd University of Petroleum and Minerals, Saudi Arabia, for his Ph.D. study at Texas A&M University. This work was supported by the DOE Advanced Gas Turbine Systems Research (AGTSR) program through project number SR-094. The support of the above institutions is greatly appreciated.

Nomenclature

- D = hydraulic diameter (m)
- e = rib height (m)
- h = heat transfer coefficient (W/m^2K)
- k = thermal conductivity of coolant (W/mK)
- Nu = local Nusselt number, hD/k
- Nu_o = Nusselt number in fully-developed turbulent non-rotating tube flow with smooth wall
- P = rib pitch (m)
- Pr = Prandtl number
- q_{net} = net heat at wall (W)
- A = surface area of the copper plate (m^2)
- R = radial distance from axis of rotation to heated test section's mean radius
- Re = Reynolds number, $\rho VD/\mu$
- R_o = rotation number, $\Omega D/V$
- T_{bx} = local coolant temperature (degC)
- T_{bi} = coolant temperature at inlet (degC)
- T_w = wall temperature (degC)
- V = bulk velocity in streamwise direction (m/s)
- β = angle of channel orientation with respect to the axis of rotation
- Ω = rotational speed (rad/s)
- ω = rotational speed (rpm)
- α = rib angle
- μ = dynamic viscosity of coolant (Pa-s)
- ρ = density of coolant (kg/m^3)
- $\Delta\rho/\rho$ = inlet coolant-to-wall density ratio, $(T_w - T_{bi})/T_w$

References

- [1] Metzger, D. E., and Sahn, M. K., 1986, "Heat Transfer Around Sharp 180 deg Turns in Smooth Rectangular Channels," *ASEM J. Heat Transfer*, **113**, pp. 500-506.
- [2] Fan, C. S., and Metzger, D. E., 1987, "Effects of Channel Aspect Ratio on

- Heat Transfer in Rectangular Passage Sharp 180 deg Turn," ASME Paper No. 87-GT-113.
- [3] Han, J. C., and Park, J. S., 1988, "Developing Heat Transfer in Rectangular Channels With Rib Turbulators," *Int. J. Heat Mass Transf.*, **31**(1), pp. 183–195.
- [4] Han, J. C., Zhang, Y. M., and Lee, C. P., 1991, "Augmented Heat Transfer in Square Channels With Parallel, Crossed, and V-Shaped Angled Ribs," *ASME J. Heat Transfer*, **113**, pp. 590–596.
- [5] Taslim, M. E., Li, T., and Kercher, D. M., 1994, "Experimental Heat Transfer and Friction in Channels Roughened With Angled V Shaped and Discrete Ribs on Two Opposite Walls," ASME Paper 94-GT-163.
- [6] Ekkad, S. V., and Han, J. C., 1997, "Detailed Heat Transfer Distribution in Two-Pass Square Channels With Rib Turbulators," *Int. J. Heat Mass Transf.*, **40**(11), pp. 2525–2537.
- [7] Kiml, R., Mochizuki, S., and Murata, A., 2001, "Heat Transfer Enhancement Mechanism in a Rectangular Passage with V- and Λ -Shaped Ribs," *Journal of Flow Visualization and Image Processing*, **8**, pp. 51–68.
- [8] Wagner, J. H., Johnson, B. V., and Hajek, T. J., 1991, "Heat Transfer in Rotating Passage With Smooth Walls and Radial Outward Flow," *ASME J. Turbomach.*, **113**, pp. 42–51.
- [9] Wagner, J. H., Johnson, B. V., and Kooper, F. C., 1991b, "Heat Transfer in Rotating Serpentine Passage With Smooth Walls," *ASME J. Turbomach.*, **113**(3), pp. 321–330.
- [10] Johnson, B. V., Wagner, J. H., Steuber, G. D., and Yeh, F. C., 1994, "Heat Transfer in Rotating Serpentine Passage With Trips Skewed to the Flow," *ASME J. Turbomach.*, **116**, pp. 113–123.
- [11] Johnson, B. V., Wagner, J. H., Steuber, G. D., and Yeh, F. C., 1994, "Heat Transfer in Rotating Serpentine Passage With Selected Model Orientations for Smooth or Skewed Trip Walls," *ASME J. Turbomach.*, **116**, pp. 738–744.
- [12] Han, J. C., Zhang, Y. M., and Kalkuehler, K., 1993, "Uneven Wall Temperature Effect on Local Heat Transfer in a Rotating Two-Pass Square Channel With Smooth Walls," *ASME J. Heat Transfer*, **115**(4), pp. 912–920.
- [13] Zhang, Y. M., Han, J. C., Parsons, J. A., and Lee, C. P., 1995, "Surface Heating Effect on Local Heat Transfer in a Rotating Two-Pass Square Channel With 60 deg Angled Rib Turbulators," *ASME J. Turbomach.*, **117**, pp. 272–280.
- [14] Parsons, J. A., Han, J. C., and Zhang, Y. M., 1994, "Wall Heating Effect on Local Heat Transfer in a Rotating Two-Pass Square Channel With 90 deg Rib Turbulators," *Int. J. Heat Mass Transf.*, **37**(9), pp. 1411–1420.
- [15] Parsons, J. A., Han, J. C., and Zhang, Y. M., 1995, "Effects of Model Orientation and Wall Heating Condition on Local Heat Transfer in a Rotating Two-Pass Square Channel With 90 deg Rib Turbulators," *Int. J. Heat Mass Transf.*, **38**(7), pp. 1151–1159.
- [16] Dutta, S., and Han, J. C., 1996, "Local Heat Transfer in Rotating Smooth and Ribbed Two-Pass Square Channels With Three Channel Orientations," *ASME J. Heat Transfer*, **118**, pp. 578–584.
- [17] Dutta, S., and Han, J. C., and Lee, C. P., 1996, "Local Heat Transfer in a Rotating Two-Pass Ribbed Triangular Duct With Two Model Orientations," *Int. J. Heat Mass Transf.*, **39**, pp. 707–715.
- [18] Taslim, M. E., Rahman, A., and Spring, S. D., 1991, "An Experimental Investigation of Heat Transfer Coefficients in a Spanwise Rotating Channel With Two Opposite Rib-Roughened Walls," *ASME J. Turbomach.*, **113**, pp. 75–82.
- [19] Taslim, M. E., Bondi, L. A., and Kercher, D. M., 1991b, "An Experimental Investigation of Heat Transfer in an Orthogonally Rotating Channel Roughened With 45 deg Criss-Cross Ribs on Two Opposite Walls," *ASME J. Turbomach.*, **113**, pp. 346–353.
- [20] Prabhu, S. V., and Vedula, R. P., 1997, "Pressure Drop Distribution in a Rotating Rectangular Channel With One Ribbed Surface," *ASME Paper No. 97-AA-118*.
- [21] Park, C. W., Yoon, C., and Lau, S. C., 2000, "Heat (Mass) Transfer in a Diagonally Oriented Rotating Two-Pass Channel with Rib-Roughened Walls," *ASME J. Heat Transfer*, **122**, pp. 208–211.
- [22] Azad, G. M. S., Uddin, M. J., Han, J. C., Moon, H. K., and Glezer, B., 2002, "Heat Transfer in Two-Pass Rectangular Rotating Channels with 45 deg Parallel and Crossed rib Turbulators," *ASME J. Turbomach.*, **124**, pp. 251–259.
- [23] Han, J. C., Dutta, S., and Ekkad, S. V., 2000, *Gas Turbine Heat Transfer and Cooling Technology*, Taylor & Francis, Inc., New York, ISBN #1-56032-841-X.
- [24] Kline, S. J., and McClintock, F. A., 1953, "Describing Uncertainties in Single-Sample Experiments," *Mech. Eng. (Am. Soc. Mech. Eng.)*, **75**, pp. 3–8.
- [25] Al-Qahtani, M., Jang, Y., Chen, H., and Han, J. C., 2002, "Prediction of Flow and Heat Transfer in Rotating Two-Pass Rectangular Channels with 45 deg Rib Turbulators," *ASME J. Turbomach.*, **124**, pp. 242–250.